

# Spectroscopy of $^{54}\text{Ti}$ and the systematic behavior of low energy octupole states in Ca and Ti isotopes

L. A. Riley,<sup>1</sup> M. L. Agiorgousis,<sup>1</sup> T.R. Baugher,<sup>2,3</sup> D. Bazin,<sup>2</sup> R.L. Blanchard,<sup>1</sup> M. Bowry,<sup>2,3</sup> P. D. Cottle,<sup>4</sup> F. G. DeVone,<sup>1</sup> A. Gade,<sup>2,3</sup> M. T. Glowacki,<sup>1</sup> K. W. Kemper,<sup>4</sup> J.S. Kustina,<sup>1</sup> E. Lunderberg,<sup>2,3</sup> D. M. McPherson,<sup>4</sup> S. Noji,<sup>2,5</sup> J. Piekarewicz,<sup>4</sup> F. Recchia,<sup>2,\*</sup> B. V. Sadler,<sup>1</sup> M. Scott,<sup>2,3</sup> D. Weisshaar,<sup>2</sup> and R. G. T. Zegers<sup>2,3,5</sup>

<sup>1</sup>*Department of Physics and Astronomy, Ursinus College, Collegeville, PA 19426, USA*

<sup>2</sup>*National Superconducting Cyclotron Laboratory, Michigan State University, East Lansing, MI, 48824, USA*

<sup>3</sup>*Department of Physics and Astronomy, Michigan State University, East Lansing, MI, 48824, USA*

<sup>4</sup>*Department of Physics, Florida State University, Tallahassee, FL 32306, USA*

<sup>5</sup>*Joint Institute for Nuclear Astrophysics - Center for the Evolution of the Elements, Michigan State University, East Lansing, MI 48824, USA*

(Dated: October 10, 2018)

Excited states of the  $N = 32$  nucleus  $^{54}\text{Ti}$  have been studied, via both inverse-kinematics proton scattering and one-neutron knockout from  $^{55}\text{Ti}$  by a liquid hydrogen target, using the GRETINA  $\gamma$ -ray tracking array. Inelastic proton-scattering cross sections and deformation lengths have been determined. A low-lying octupole state has been tentatively identified in  $^{54}\text{Ti}$  for the first time. A comparison of  $(p, p')$  results on low-energy octupole states in the neutron-rich Ca and Ti isotopes with the results of Random Phase Approximation calculations demonstrates that the observed systematic behavior of these states is unexpected.

## I. INTRODUCTION

In atomic nuclei, collective low-energy octupole vibrations - like other collective vibrations - are coherent sums of one particle-one hole excitations. Of course, to contribute to octupole vibrations the particle-hole excitations must have  $J^\pi = 3^-$ . For low-energy octupole states, that requires that a nucleon be promoted from a common parity orbit to an opposite parity high- $j$  orbit that has been depressed in energy due to the spin-orbit force.

The occupation of the orbits involved in these particle-hole excitations affects the systematic behavior of the octupole states in a predictable way across most of the nuclear landscape. For example, the low-energy octupole state in the  $N = Z = 20$  isotope  $^{40}\text{Ca}$  is composed primarily of excitations of both protons and neutrons from  $sd$  orbits to the  $f_{7/2}$  orbit. When neutrons are added to  $^{40}\text{Ca}$ , they occupy the  $f_{7/2}$  neutron orbit, blocking  $J^\pi = 3^-$  excitations of neutrons from the  $sd$  orbits. Therefore, fewer particle-hole excitations are available to contribute to the low-energy octupole state. At  $N = 28$ , the  $f_{7/2}$  neutron orbit is full and neutron contributions to the low-energy octupole state are suppressed. As a result, the energy of the  $3_1^-$  state increases from 3737 keV in  $^{40}\text{Ca}$  to 4507 keV in  $^{48}\text{Ca}$ . The  $E3$  excitation strength to the  $3_1^-$  state as measured by electron scattering decreases from 28(3) single particle units in  $^{40}\text{Ca}$  to 9(2) single particle units in  $^{48}\text{Ca}$ .

By the same reasoning, adding neutrons to  $^{48}\text{Ca}$  should provide additional particle-hole contributions to the low-energy octupole state as excitations from the  $p_{3/2}$  neutron orbit to the  $g_{9/2}$  orbit become available. We would

expect that this would result in a decrease in the energy of the low-energy octupole state and an increase in  $E3$  strength as the neutron number increases above  $^{48}\text{Ca}$ . However, a systematic experimental study of  $3_1^-$  states in the neutron-rich Ca isotopes by Riley *et al.* [1] found that is not the case. Instead, the  $(p, p')$  strength to the  $3_1^-$  states in  $^{50,52}\text{Ca}$  are equal to that in  $^{48}\text{Ca}$ , within experimental uncertainties.

Here we report on a spectroscopic study of the exotic neutron-rich isotope  $^{54}\text{Ti}$  via the reaction  $(p, p')$  and knockout of a neutron from  $^{55}\text{Ti}$ . Excited states of  $^{54}\text{Ti}$  have been studied before via deep inelastic reactions of  $^{48}\text{Ca}$  on  $^{208}\text{Pb}$  [2] and  $^{238}\text{U}$  [3] targets, beta decay [4, 5], and Coulomb excitation [6]. However, these reactions do not favorably populate low-lying collective octupole states. The measurements of the present work allowed us to determine the energy and strength of the  $3_1^-$  state of  $^{54}\text{Ti}$  and to examine the systematic behavior of octupole states in the neutron-rich Ca and Ti isotopes.

To provide a theoretical context for these experimental results, we also report the results of a Random Phase Approximation (RPA) study of low-energy octupole states in the Ca and Ti isotopes.

## II. EXPERIMENTAL DETAILS

The experiment was performed at the Coupled-Cyclotron Facility of the National Superconducting Cyclotron Laboratory at Michigan State University (NSCL). The secondary beam was produced by the fragmentation of a 130 MeV/u  $^{76}\text{Ge}$  primary beam in a 376 mg/cm<sup>2</sup>  $^9\text{Be}$  production target and separated by the A1900 fragment separator [7]. The momentum acceptance of the A1900 was 3%. A 45 mg/cm<sup>2</sup> aluminum achromatic wedge was used to further purify the sec-

\* Dipartimento di Fisica e Astronomia Galileo Galilei, Università degli Studi di Padova, I-35131 Padova, Italy

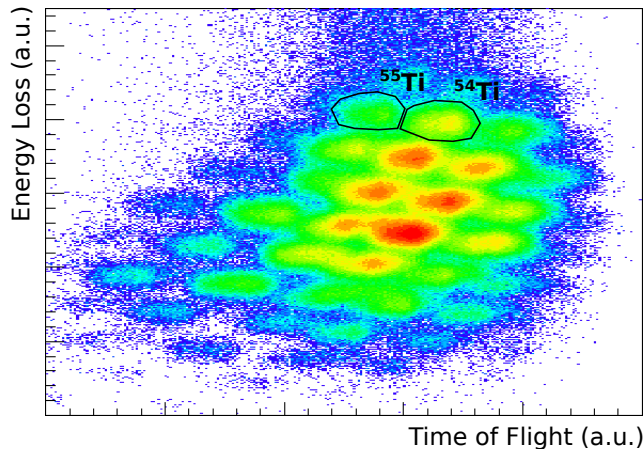


FIG. 1. (Color online) Energy loss in a Si PIN diode vs. time of flight from the A1900 extended focal plane to the S800 object scintillator of the incoming beam used for particle identification.

ondary beam by  $Z$ .

Secondary beam particles were identified upstream of the reaction target by energy loss in a silicon surface barrier detector and by time of flight from the A1900 extended focal plane to the S800 object scintillator. The incoming particle identification spectrum is shown in Figure 1. The beam then passed through the NSCL/Ursinus College Liquid Hydrogen Target, based on the design of Ryuto et al. [8]. The target was installed at the target position of the S800 magnetic spectrograph [9]. Beam-like reaction products were identified downstream of the target by energy loss in the S800 ion chamber and time of flight from the S800 object scintillator to a scintillator in the focal plane of the S800. The secondary beam contained components spanning the range  $14 \leq Z \leq 23$ , including  $^{54,55}\text{Ti}$ . A total of  $1.59 \times 10^7$   $^{54}\text{Ti}$  and  $8.71 \times 10^6$   $^{55}\text{Ti}$  particles passed through the target during the measurement at rates of 39 particles/s and 21 particles/s, respectively.

The liquid hydrogen was contained by a cylindrical aluminum target cell with 125  $\mu\text{m}$  Kapton entrance and exit windows mounted on a cryocooler. The nominal target thickness was 30 mm. The target cell and cryocooler were surrounded by a 1 mm thick aluminum radiation shield with entrance and exit windows covered by 5  $\mu\text{m}$  aluminized Mylar foil. The temperature and pressure of the target cell was 16.00(25) K and 868(10) Torr throughout the experiment. The variation in the temperature and pressure of the target cell correspond to a 0.3 % uncertainty in target density.

The Kapton windows of the target cell bulged significantly due to the pressure difference between the cell and the evacuated beam line. The effective thickness of the target was determined to be 258  $\text{mg}/\text{cm}^2$  by fitting GEANT4 simulations of the beam passing through the target to the measured kinetic energy distribution of the outgoing reaction products as described in Ref. [10].

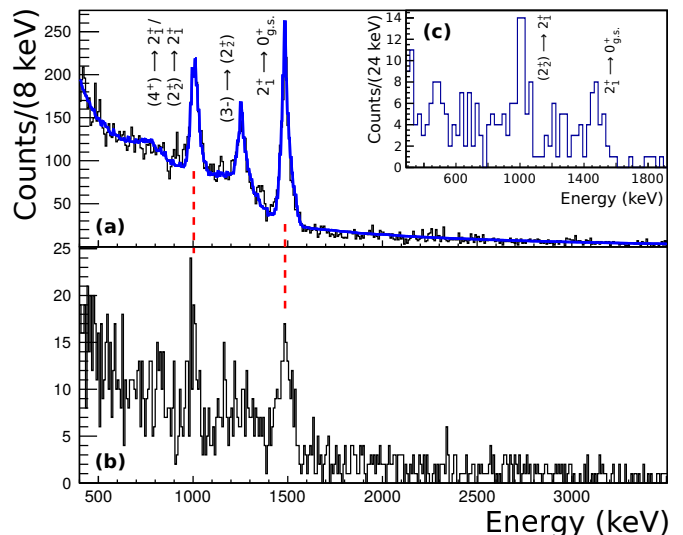


FIG. 2. (Color online) Projectile-frame  $\gamma$ -ray spectra of  $^{54}\text{Ti}$  measured via (a) inverse-kinematics proton scattering and (b) one-neutron knockout from  $^{55}\text{Ti}$ . The solid curve is the fit of GEANT4 simulations to the spectrum obtained from  $(p, p')$ . (c) Spectrum of  $\gamma$  rays obtained from  $(p, p')$  gated on the 1264-keV  $\gamma$  ray.

The mid-target beam energy was 91.5 MeV/nucleon.

The GRETTINA  $\gamma$ -ray tracking array [11, 12], consisting of 28 36-fold segmented high purity germanium crystals packaged in seven clusters of four crystals each, was installed at the pivot point of the S800. In order to accommodate the liquid hydrogen target, the array was mounted on the north half of the mounting shell with two modules centered at  $58^\circ$ , four at  $90^\circ$ , and one at  $122^\circ$  with respect to the beam axis.

### III. EXPERIMENTAL RESULTS

The Doppler-corrected spectrum of  $\gamma$  rays measured in coincidence with incoming and outgoing  $^{54}\text{Ti}$  particles, corresponding to the  $(p, p')$  reaction, is shown in panel (a) of Figure 2. Panel (b) of the figure shows the  $\gamma$ -ray spectrum measured in coincidence with incoming  $^{55}\text{Ti}$  and outgoing  $^{54}\text{Ti}$  particles, corresponding to the one-neutron knockout reaction. The average projectile speed used in Doppler reconstruction was  $v/c = 0.41$ . The  $\gamma$  rays at 1495, 1002, and 1021 keV correspond to transitions observed in the  $\beta$ -decay study of Crawford et al [5]. An additional  $\gamma$ -ray at 1264 keV is observed for the first time. The  $\gamma$ -ray spectrum from  $(p, p')$  measured in coincidence with the 1264-keV  $\gamma$  ray is shown in panel (c) of Figure 2. On this basis, we identify the 1264-keV transition as part of a cascade involving the 1495-keV  $2_1^+ \rightarrow 0_{g.s.}^+$  transition and one of the transitions in the unresolved 1002/1021-keV doublet.

The solid curve overlaid on the  $\gamma$ -ray spectrum collected via  $(p, p')$  in panel (a) of Figure 2 is a fit of GEANT4

TABLE I. Level energies, spins and parities,  $\gamma$ -ray energies, and branching ratios (BR) from Ref. [5],  $\gamma$ -ray energies, intensities relative to that of the  $2_1^+ \rightarrow 0_{g.s.}^+$  transition, and branching ratios (BR), and cross sections from the present work.

$E_{\text{level}}$ [keV]	$J^\pi$ [ $\hbar$ ]	Ref. [5]		Present work			
		$E_\gamma$ [keV]	BR [%]	$E_\gamma$ [keV]	$I_\gamma$ [%]	BR [%]	$\sigma$ [mb]
1495.0(3)	$2_1^+$	1495.0(3)		1495(2)	100		8.7(8)
2497.4(4)	$(4^+)$	1002.4(3)		1000(3)	20(3)		3.3(4)
2517.1(3)	$(2_2^+)$	1020.8(4)	64(14)	1022(3)	27(3)	>84	<0.7
		2517.5(3)	36(7)	2517	<6	<16	
3780(3)	$(3^-)$			1264(3)	29(3)		4.9(4)

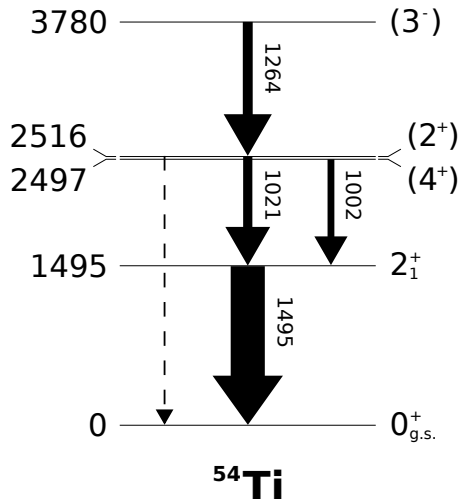


FIG. 3. Partial level scheme of  $^{54}\text{Ti}$  showing levels populated in the present work. Arrow widths are proportional to the  $\gamma$ -ray intensities measured in the  $(p, p')$  reaction.

simulations of the response of GRETTINA to the observed  $\gamma$  rays and prompt and non-prompt background using the method described in Ref. [10]. The  $\gamma$ -ray energies and intensities extracted from the fits are listed in Table I along with the branching ratios. Also included are level energies,  $\gamma$ -ray energies and branching ratios from Ref. [5].

The 2517-keV ( $2_2^+ \rightarrow 0_{g.s.}^+$ ) transition observed in the beta-decay study of Crawford et al. [5] was included in the fit. The best-fit yield of this  $\gamma$  ray is consistent with zero. The upper limit on its intensity in Table I is based on the statistical uncertainty from the fit. A fit assuming the branching ratio to the 2517-keV transition observed in Ref. [5] is not consistent with our spectrum.

A partial level scheme for  $^{54}\text{Ti}$  including states populated in the present work is shown in Figure 3. The level scheme, with the exception of the new state at 3780 keV, corresponds to that established in Ref. [5]. We place the 1264-keV transition feeding the ( $2_2^+$ ) state at 2497 keV on the basis that the measured relative intensity of the 1264-keV  $\gamma$  ray is significantly greater than that of the 1002-keV  $\gamma$  ray. Using this level scheme, we applied feeding corrections to the measured  $\gamma$ -ray yields to determine the cross sections for populating excited states via proton

scattering that are listed in Table I.

We make a tentative assignment of  $J^\pi = 3^-$  to the state at 3780 keV because it has a large  $(p, p')$  cross section, it decays to the ( $2_2^+$ ) state and it is in the broad energy range associated with low-energy octupole states in this mass region [1, 13].

The absence of the 1264-keV  $\gamma$  ray from the neutron knockout spectrum is consistent with the  $3_1^-$  assignment for the 3780-keV state for reasons that will be explained below.

We used the coupled-channels code ECIS95 [14] and the global optical potential of Ref. [15] to determine deformation lengths from our measured cross sections for inelastic scattering to the  $2_1^+$ ,  $3^-$  and  $4_1^+$  states of  $\delta_2 = 0.93(4)$  fm,  $\delta_3 = 0.76(3)$  fm and  $\delta_4 = 0.67(4)$  fm.

#### IV. RANDOM PHASE APPROXIMATION CALCULATIONS

The distribution of isoscalar  $E3$  strength is computed in a relativistic random phase approximation (RPA) using three effective interactions that have been calibrated to the properties of finite nuclei: NL3 [16, 17], FSUGold [18], and FSUGarnet [19]. The development of FSUGold used NL3 as a starting point, and FSUGarnet is a refinement of FSUGold that has been fitted to a few giant monopole energies and to well-established properties of neutron stars [20]. Moreover, FSUGarnet predicts that the isotopic chain in oxygen can be made to terminate at  $^{24}\text{O}$ , as has been observed experimentally [21]. The parameters for the three relativistic models are tabulated in [22].

The implementation of the RPA formalism adopted here is rooted in a non-spectral approach that allows for an exact treatment of the continuum without any reliance on discretization. This is particularly critical in the case of weakly-bound nuclei with single-particle orbits near the continuum. The discretization of the continuum is neither required nor admitted. The relativistic RPA formalism as implemented here has been reviewed extensively in earlier publications; see for example Refs. [23, 24] and references contained therein. In the context of the isoscalar monopole response of the neutron-rich calcium isotopes, the details of the formalism are

described in [22].

The RPA calculations were performed for  $^{40,42,44,46,48,50,52}\text{Ca}$  and  $^{50,52,54}\text{Ti}$ . Figure 4 shows the  $E3$  strength distributions calculated for  $^{40,42,44,46,48}\text{Ca}$  using FSUGarnet, which is the most refined of the three interactions used here. The first feature to notice is that in each of these isotopes there is a concentration of strength below 6 MeV. This is the Low-Energy Octupole State (LEOS) that is sometimes - but not always - concentrated in the  $3_1^-$  state.

Above 6 MeV, a second concentration of  $E3$  strength can be seen - the Low-Energy Octupole Resonance (LEOR) - which occurs throughout the Periodic Table at energies near  $(31 \text{ MeV})/A^{1/3}$  [25].

Both the LEOS and LEOR are composed of  $1\hbar\omega$  one particle-one hole excitations. However, the LEOS is composed of excitations to the high-spin “intruder” orbit that is pushed down by the spin-orbit force from the major shell  $1\hbar\omega$  above. The LEOR includes excitations to the rest of the major shell  $1\hbar\omega$  above.

For  $N < 28$  Ca isotopes, the LEOS is composed mostly of excitations of both protons and neutrons from the  $sd$  shell to the  $f_{7/2}$  orbit. The LEOR is mostly composed of excitations from the  $sd$  orbits to the  $p_{3/2}$ ,  $p_{1/2}$  and  $f_{5/2}$  orbits.

In Figure 4, the RPA calculation clearly shows the behavior we expect in the simplest picture of octupole vibrations. The maximum number of excitations from the  $sd$  shell to the  $f_{7/2}$  orbits is available in  $N = Z = 20$   $^{40}\text{Ca}$ . Therefore, the strength of the LEOS is at a maximum and the energy of the LEOS is at a minimum in that isotope. As neutrons are added to  $^{40}\text{Ca}$ , the increasing occupation of the  $f_{7/2}$  neutron orbit blocks neutron contributions to the LEOS. As a result, the strength of the LEOS decreases and its energy increases until  $^{48}\text{Ca}$  is reached and the LEOS energy reaches a maximum and the  $E3$  strength reaches a minimum.

## V. SYSTEMATIC BEHAVIOR OF LOW-ENERGY OCTUPOLE STATES IN Ca AND Ti ISOTOPES

Before we examine the results of the calculations for the Ti isotopes, including  $^{54}\text{Ti}$  which is the focus of the present work, we compare the results of the RPA calculations for Ca isotopes to the data. Figure 5 compares the RPA results using the three models to the energies and  $E3$  strengths of the LEOS in  $^{40,42,44,46,48}\text{Ca}$ . The energies of states shown in Figure 5 are taken from compilations [26–30]. The  $E3$  strengths are from electron scattering (also taken from the compilations), which provides a uniform data set for these isotopes. The points labeled “All  $3^-$ ” are explained in the next paragraph.

If we only look at the  $3_1^-$  states in Figure 5, we see an energy trend that we do not expect for the LEOS. As neutrons are added to  $^{40}\text{Ca}$ , the energy of the  $3_1^-$  state decreases. However, the electron scattering mea-

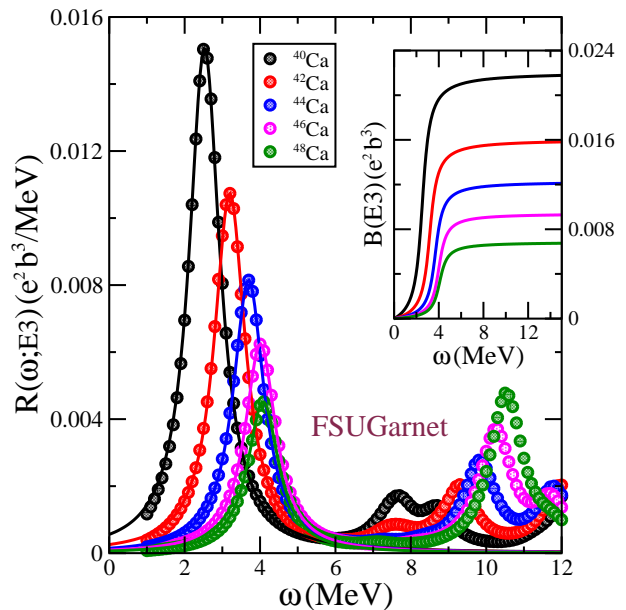


FIG. 4. (Color online)  $E3$  strength distributions for  $^{40,42,44,46,48}\text{Ca}$  calculated with the RPA.

surements revealed other  $3^-$  states in the LEOS energy range (below 6 MeV) in  $^{42,44,48}\text{Ca}$ . That is, it appears that the LEOS has fragmented in these three isotopes (there are no electron scattering results for  $^{46}\text{Ca}$ ). If instead of only considering the  $3_1^-$  states we say that the LEOS energies are the centroids of the strength as seen in electron scattering, then the decrease in energy does not occur, as indicated with “All  $3^-$ ” in Figure 5.

Figure 5 also shows the LEOS  $E3$  strength results both without accounting for LEOS fragmentation (that is, only the  $3_1^-$  states) and including the LEOS fragments observed in electron scattering. For both LEOS energies and strengths, the calculations qualitatively reproduce the trends in the data for  $^{40,42,44,46,48}\text{Ca}$ .

The RPA strength distributions for  $^{48,50,52}\text{Ca}$  are shown in Figure 6 and compared to the RPA result for  $^{40}\text{Ca}$ . The RPA calculation predicts that when neutrons are added to  $^{48}\text{Ca}$  the  $E3$  strength of the LEOS increases quickly and the energy declines. The calculated  $E3$  strength increases by more than a factor of three from  $^{48}\text{Ca}$  to  $^{52}\text{Ca}$ , reaching a value comparable to that in  $^{40}\text{Ca}$ .

The origin of the increase in  $E3$  strength and decrease in LEOS energy as neutrons are added to  $^{48}\text{Ca}$  in the RPA calculation is straightforward to understand. The neutrons added to  $^{48}\text{Ca}$  mostly occupy the  $p_{3/2}$  orbit, adding one neutron-one neutron hole excitations to the  $g_{9/2}$  orbit for the LEOS wavefunction. We note, however, that the  $g_{9/2}$  orbit is predicted to be in the continuum, so the non-spectral approach adopted here offers a distinct advantage over the spectral approach.

Figure 7 compares the RPA results with data on octupole states in  $^{48,50,52}\text{Ca}$  from Ref. [1], in which these isotopes were studied via the  $(p,p')$  reaction in inverse

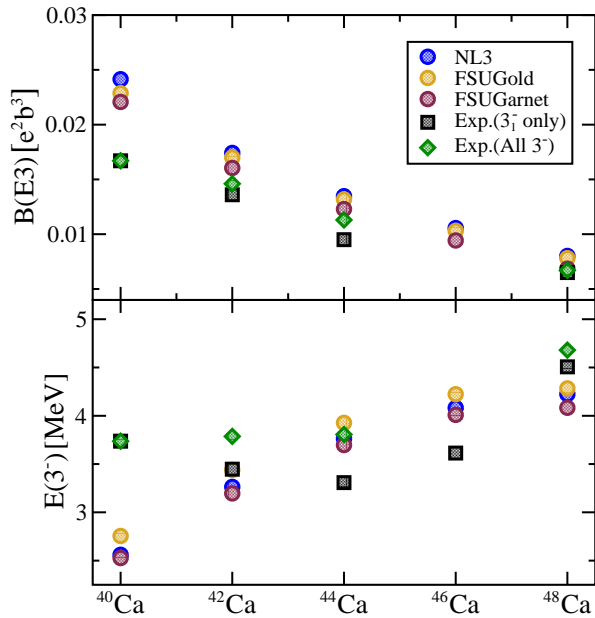


FIG. 5. (Color online) Comparison of the systematic behavior of RPA calculations of LEOS energy and  $E3$  strength for  $^{40,42,44,46,48}\text{Ca}$  with data. The black squares show the energies of the  $3_1^-$  states and the  $B(E3; \uparrow)$  values for the  $3_1^-$  states from electron scattering. The green diamonds show the total  $E3$  strength for all  $3^-$  states observed in electron scattering below 6 MeV, and the centroids of this  $E3$  strength.

kinematics - providing a uniform data set for all three nuclei. The data show that the energies of the  $3_1^-$  states drop from 4.5 MeV in  $^{48}\text{Ca}$  to 4.0 MeV in  $^{50,52}\text{Ca}$ . The  $E3$  strength for exciting the  $3_1^-$  states stays constant within experimental uncertainty. The  $B(E3; \uparrow)$  values are calculated from the  $\delta_3$  values in Ref. [1] using the prescription given in Ref. [13] and the real radius parameters from Ref. [15]. The  $E3$  strength is constant, in contrast with the RPA prediction that rises sharply. So the experimental results for  $^{50,52}\text{Ca}$  can be considered unexpected.

However, it is important to note that the radioactive beam experiment from which the results in Figure 7 were extracted only yielded the observation of a single  $3^-$  state in each nucleus. It is possible that the LEOS is fragmented in  $^{50,52}\text{Ca}$  and that this fragmentation was not observed in the experiment.

Figure 8 shows the results of RPA calculations for  $^{48}\text{Ca}$  and  $^{50,52,54}\text{Ti}$ . The calculations predict that the  $N = 28$  isotope  $^{50}\text{Ti}$  has a somewhat smaller  $E3$  strength in the LEOS than  $^{48}\text{Ca}$  because the two additional protons occupy the  $f_{7/2}$  orbit and block some of the one proton-one hole excitations from the  $sd$  shell that contribute to the LEOS in  $^{48}\text{Ca}$ . However, a much larger change to the  $E3$  strength occurs when neutrons are added to  $^{54}\text{Ti}$ : the calculation predicts that the  $E3$  strength in  $^{54}\text{Ti}$  is four times higher than in  $^{50}\text{Ti}$ . As in the  $N > 28$  Ca isotopes, that rapid increase in the calculated  $E3$  strength is driven by the occupation of the  $p_{3/2}$  neutron orbit which

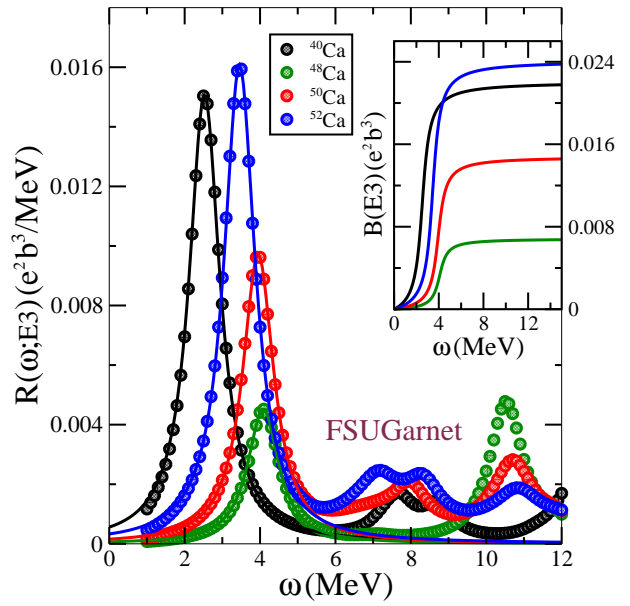


FIG. 6. (Color online)  $E3$  strength distributions for  $^{40,48,50,52}\text{Ca}$  calculated with the RPA.

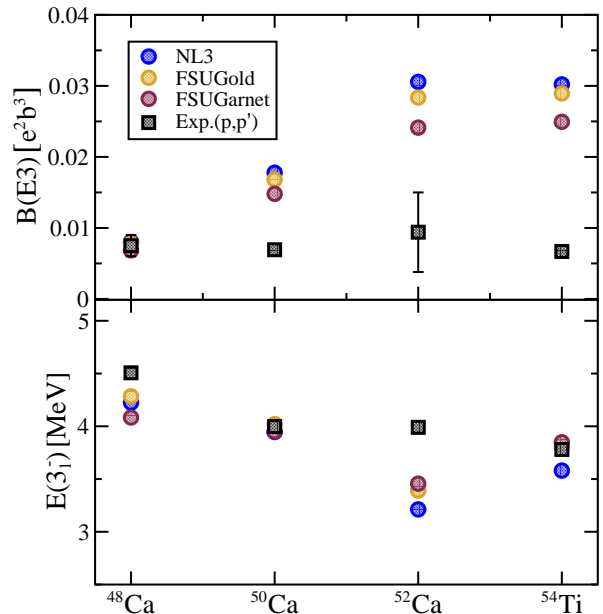


FIG. 7. (Color online) Comparison of the systematic behavior of RPA calculations of LEOS energy and  $E3$  strength for  $^{48,50,52}\text{Ca}$  and  $^{54}\text{Ti}$  with data. The black squares show the energies of the  $3_1^-$  states and the  $B(E3; \uparrow)$  values for the  $3_1^-$  states from proton scattering in inverse kinematics (Ref. [1] and the present work).

makes available one neutron-one hole excitations to the unbound  $g_{9/2}$  orbit.

However, the present  $(p, p')$  results show that the  $E3$  strength to the  $3_1^-$  state in  $^{54}\text{Ti}$  is approximately equal to the corresponding strength in  $^{48}\text{Ca}$ , as shown in Figure 7. Once again, the calculations can be understood in a



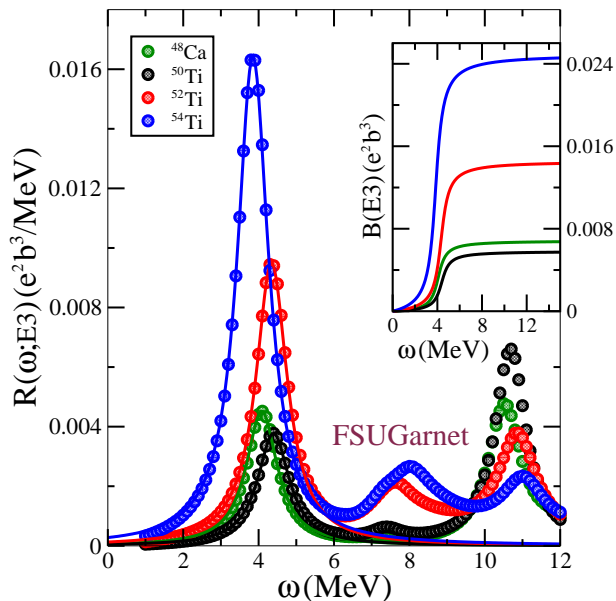


FIG. 8. (Color online)  $E3$  strength distributions for  $^{48}\text{Ca}$  and  $^{50,52,54}\text{Ti}$  calculated with the RPA.

straightforward way and we can conclude that the systematic behavior revealed by the state is unexpected unless an unobserved strong fragmentation of the strength occurs.

This explanation of the predicted role of the  $p_{3/2}$ - $g_{9/2}$  neutron-neutron hole contribution to the  $3_1^-$  state in  $^{54}\text{Ti}$  provides an explanation for the absence of the  $3_1^-$  state from the  $^{55}\text{Ti}$  knockout spectrum. The neutron knockout reaction would only populate the  $3_1^-$  state if the ground state of  $^{55}\text{Ti}$  has a neutron in the  $g_{9/2}$  orbit. In the ground state of  $^{55}\text{Ti}$ , the neutrons occupy the  $fp$  orbits, so the knockout reaction cannot populate the  $3_1^-$  state.

The fragmentation of the LEOS in  $^{42,44}\text{Ca}$  may suggest an explanation for the anomalous behavior of  $3_1^-$  states in  $^{50,52}\text{Ca}$  and  $^{54}\text{Ti}$ . The challenging nature of the exotic beam experiments reported here make it possible that fragments of the LEOS - particularly those lying higher in energy than the  $3_1^-$  states reported here and in Ref. [1] - were not detected. If the LEOS is fragmented in  $^{50,52}\text{Ca}$  and  $^{54}\text{Ti}$ , the total  $E3$  strength to the LEOS

might be considerably larger than we have observed in the  $3_1^-$  states of these nuclei.

It is worth noting that  $^{42,44}\text{Ca}$  are not the only nuclei in this mass region in which the LEOS is significantly fragmented. Higashi *et al.* [31] used 65 MeV proton scattering to observe the fragmentation of the LEOS in stable  $^{46,48}\text{Ti}$ . We can conclude that the fragmentation of the LEOS is the most likely explanation for the large discrepancies between the experimental  $(p, p')$  results for  $3_1^-$  states in  $^{50,52}\text{Ca}$  and  $^{54}\text{Ti}$  and the RPA calculations presented here.

## VI. SUMMARY

The spectroscopy of  $^{54}\text{Ti}$  has been performed with two reactions in the same target - inelastic proton scattering in inverse kinematics and one-neutron knockout from  $^{55}\text{Ti}$ . A state at 3780 keV has been tentatively identified as the  $3_1^-$  state. Deformation lengths have been extracted from the  $(p, p')$  data for the  $2_1^+$ ,  $4_1^+$  and  $3_1^-$  states.

RPA calculations have been performed for the LEOS in  $^{40,42,44,46,48,50,52}\text{Ca}$  and  $^{50,52,54}\text{Ti}$ . The observed  $E3$  strength in the  $3_1^-$  states of  $^{50,52}\text{Ca}$  and  $^{54}\text{Ti}$  is considerably smaller than the predicted values. This may be because the LEOS is fragmented in these isotopes. A more sensitive experiment to detect other  $3^-$  states in these isotopes should be performed to determine whether fragmentation causes the discrepancy between the data and the calculation or whether the strength of the LEOS is quenched.

## ACKNOWLEDGMENTS

This work was supported by the National Science Foundation under Grant Nos. PHY-1617250, PHY-1303480, PHY-1064819, PHY-1565546, and 1401574. One of us (JP) is supported by the U.S. Department of Energy Office of Science, Office of Nuclear Physics under Award Number DE-FD05-92ER40750. GREINA was funded by the US DOE - Office of Science. Operation of the array at NSCL was supported by NSF under Cooperative Agreement PHY-1102511(NSCL) and DOE under grant DE-AC02-05CH11231(LBNL). We also thank T.J. Carroll for the use of the Ursinus College Parallel Computing Cluster, supported by NSF grant no. PHY-1205895.

- 
- [1] L. A. Riley, D. M. McPherson, M. L. Agiorgousis, T. R. Baugher, D. Bazin, M. Bowry, P. D. Cottle, F. G. DeVone, A. Gade, M. T. Glowacki, S. D. Gregory, E. B. Haldeman, K. W. Kemper, E. Lunderberg, S. Noji, F. Recchia, B. V. Sadler, M. Scott, D. Weisshaar, and R. G. T. Zegers, *Phys. Rev. C* **93**, 044327 (2016).
- [2] R. V. F. Janssens, B. Fornal, P. F. Mantica, B. A. Brown, R. Broda, P. Bhattacharyya, M. P. Carpenter, M. Cinausero, P. J. Daly, A. D. Davies, T. Glasmacher,

- Z. W. Grabowski, D. E. Groh, M. Honma, F. G. Kondev, W. Królás, T. Lauritsen, S. N. Liddick, S. Lunardi, N. Marginean, T. Mizusaki, D. J. Morrissey, A. C. Morton, W. F. Mueller, T. Otsuka, T. Pawlat, D. Seweryniak, H. Schatz, A. Stolz, S. L. Tabor, C. A. Ur, G. Vestri, I. Wiedenhöver, and J. Wrzesiski, *Physics Letters B* **546**, 55 (2002).
- [3] B. Fornal, S. Zhu, R. V. F. Janssens, M. Honma, R. Broda, P. F. Mantica, B. A. Brown, M. P. Carpen-

- ter, P. J. Daly, S. J. Freeman, Z. W. Grabowski, N. J. Hammond, F. G. Kondev, W. Królas, T. Lauritsen, S. N. Liddick, C. J. Lister, E. F. Moore, T. Otsuka, T. Pawlat, D. Seweryniak, B. E. Tomlin, and J. Wrzesiński, *Phys. Rev. C* **70**, 064304 (2004), copyright (C) 2010 The American Physical Society; Please report any problems to prola@aps.org.
- [4] S. N. Liddick, P. F. Mantica, R. Broda, B. A. Brown, M. P. Carpenter, A. D. Davies, B. Fornal, T. Glasmacher, D. E. Groh, M. Honma, M. Horoi, R. V. F. Janssens, T. Mizusaki, D. J. Morrissey, A. C. Morton, W. F. Mueller, T. Otsuka, J. Pavan, H. Schatz, A. Stolz, S. L. Tabor, B. E. Tomlin, and M. Wiedeking, *Phys. Rev. C* **70**, 064303 (2004).
- [5] H. L. Crawford, R. V. F. Janssens, P. F. Mantica, J. S. Berryman, R. Broda, M. P. Carpenter, N. Cieplicka, B. Fornal, G. F. Grinyer, N. Hoteling, B. P. Kay, T. Lauritsen, K. Minamisono, I. Stefanescu, J. B. Stoker, W. B. Walters, and S. Zhu, *Phys. Rev. C* **82**, 014311 (2010).
- [6] D.-C. Dinca, R. V. F. Janssens, A. Gade, D. Bazin, R. Broda, B. A. Brown, C. M. Campbell, M. P. Carpenter, P. Chowdhury, J. M. Cook, A. N. Deacon, B. Fornal, S. J. Freeman, T. Glasmacher, M. Honma, F. G. Kondev, J.-L. Lecouey, S. N. Liddick, P. F. Mantica, W. F. Mueller, H. Olliver, T. Otsuka, J. R. Terry, B. A. Tomlin, and K. Yoneda, *Phys. Rev. C* **71**, 041302 (2005), copyright (C) 2010 The American Physical Society; Please report any problems to prola@aps.org.
- [7] D. J. Morrissey, B. M. Sherrill, M. Steiner, A. Stolz, and I. Wiedenhöver, *Nucl. Instrum. Methods Phys. Res. B* **204**, 90 (2003).
- [8] H. Ryuto, M. Kunibu, T. Minemura, T. Motobayashi, K. Sagara, S. Shimoura, M. Tamaki, Y. Yanagisawa, and Y. Yano, *Nucl. Instrum. Methods Phys. Res. A* **555**, 1 (2005).
- [9] D. Bazin, J. A. Caggiano, B. M. Sherrill, J. Yurkon, and A. Zeller, *Nucl. Instrum. Methods Phys. Res. B* **204**, 629 (2003).
- [10] L. A. Riley, M. L. Agiorgousis, T. R. Baugher, D. Bazin, M. Bowry, P. D. Cottle, F. G. DeVone, A. Gade, M. T. Glowacki, K. W. Kemper, E. Lunderberg, D. M. McPherson, S. Noji, F. Recchia, B. V. Sadler, M. Scott, D. Weisshaar, and R. G. T. Zegers, *Phys. Rev. C* **90**, 011305(R) (2014).
- [11] S. Paschalis, I. Y. Lee, A. O. Macchiavelli, C. M. Campbell, M. Cromaz, S. Gros, J. Pavan, J. Qian, R. M. Clark, H. L. Crawford, D. Doering, P. Fallon, C. Lionberger, T. Loew, M. Petri, T. Stezelberger, S. Zimmermann, D. C. Radford, K. Lagergren, D. Weisshaar, R. Winkler, T. Glasmacher, J. T. Anderson, and C. W. Beausang, *Nucl. Instrum. Methods Phys. Res. A* **709**, 44 (2013).
- [12] P. Fallon, A. Gade, and I.-Y. Lee, *Annual Review of Nuclear and Particle Science* **66**, 321 (2016).
- [13] T. Kibédi and R. H. Spear, *Atomic Data and Nuclear Data Tables* **80**, 35 (2002).
- [14] J. Raynal, “Notes on ecis95,” CEA Saclay report (1995).
- [15] A. J. Koning and J.-P. Delaroche, *Nucl. Phys. A* **713**, 231 (2003).
- [16] G. A. Lalazissis, J. König, and P. Ring, *Phys. Rev. C* **55**, 540 (1997).
- [17] G. Lalazissis, S. Raman, and P. Ring, *Atomic Data and Nuclear Data Tables* **71**, 1 (1999).
- [18] B. G. Todd-Rutel and J. Piekarewicz, *Phys. Rev. Lett.* **95**, 122501 (2005).
- [19] W.-C. Chen and J. Piekarewicz, *Physics Letters B* **748**, 284 (2015).
- [20] W.-C. Chen and J. Piekarewicz, *Phys. Rev. C* **90**, 044305 (2014).
- [21] M. Thoennessen, *Reports on Progress in Physics* **67**, 1187 (2004).
- [22] J. Piekarewicz, (2017), arXiv:1707.07185 [nucl-th].
- [23] J. Piekarewicz, *The European Physical Journal A* **50**, 25 (2014).
- [24] J. Piekarewicz, *Phys. Rev. C* **91**, 014303 (2015).
- [25] M. W. Kirson, *Physics Letters B* **108**, 237 (1982).
- [26] J. Chen, *Nuclear Data Sheets* **140**, 1 (2017).
- [27] J. Chen and B. Singh, *Nuclear Data Sheets* **135**, 1 (2016).
- [28] J. Chen, B. Singh, and J. A. Cameron, *Nuclear Data Sheets* **112**, 2357 (2011).
- [29] S.-C. Wu, *Nuclear Data Sheets* **91**, 1 (2000).
- [30] T. Burrows, *Nuclear Data Sheets* **107**, 1747 (2006).
- [31] A. Higashi, K. Katori, M. Fujiwara, H. Ikegami, I. Katayama, S. Morinobu, M. Tosaki, S. I. Hayakawa, N. Ikeda, and H. Miyatake, *Phys. Rev. C* **39**, 1286 (1989).